Editors' Suggestion

Origin of Magnetism in a Supposedly Nonmagnetic Osmium Oxide

S. Agrestini,[1,*] F. Borgatti,[2] P. Florio,[3] J. Frassineti,[4] D. Fiore Mosca,[5] Q. Faure,[6] B. Detlefs,[6] C. J. Sahle,[6] S. Francoual,[7] J. Choi,[1] M. Garcia-Fernandez,[1] K.-J. Zhou,[1] V. F. Mitrović,[8] P. M. Woodward,[9] G. Ghiringhelli,[3] C. Franchini,[4] F. Boscherini,[4] S. Sanna,[4] and M. Moretti Sala[3,†]

[1]*Diamond Light Source, Harwell Campus, Didcot OX11 0DE, United Kingdom*
[2]*Istituto per lo Studio dei Materiali Nanostrutturati, Consiglio Nazionale delle Ricerche (CNR-ISMN), Via P. Gobetti 101, I-40129 Bologna, Italy*
[3]*Dipartimento di Fisica, Politecnico di Milano, Piazza Leonardo da Vinci 32, I-20133 Milano, Italy*
[4]*Dipartimento di Fisica e Astronomia "A. Righi," Alma Mater Studiorum—Università di Bologna, 11 Viale C. Berti Pichat 6/2, I-40127 Bologna, Italy*
[5]*Centre de Physique Théorique, Ecole Polytechnique, CNRS, Institut Polytechnique de Paris, 91128 Palaiseau Cedex, France*
[6]*ESRF, The European Synchrotron, 71 Avenue des Martyrs, CS40220, 38043 Grenoble Cedex 9, France*
[7]*Deutsches Elektronen-Synchrotron (DESY), Notkestrasse 85, D-22607 Hamburg, Germany*
[8]*Department of Physics, Brown University, Providence, Rhode Island 02912, USA*
[9]*Department of Chemistry and Biochemistry, The Ohio State University, Columbus, Ohio 43210, USA*

(Received 23 January 2024; revised 15 April 2024; accepted 1 July 2024; published 5 August 2024)

A supposedly nonmagnetic $5d^1$ double perovskite oxide is investigated by a combination of spectroscopic and theoretical methods, namely, resonant inelastic x-ray scattering, x-ray absorption spectroscopy, magnetic circular dichroism, and multiplet ligand-field calculations. We found that the large spin-orbit coupling admixes the $5d$ t_{2g} and e_g orbitals, covalency raises the $5d$ population well above the nominal value, and the local symmetry is lower than O_h. The obtained electronic interactions account for the finite magnetic moment of Os in this compound and, in general, of $5d^1$ ions. Our results provide direct evidence of elusive Jahn-Teller distortions, hinting at a strong electron-lattice coupling.

DOI: 10.1103/PhysRevLett.133.066501

The field of spin-orbit-coupled Mott insulators has been thriving since the notion that spin-orbit interaction can induce unexpected behaviors in solids was put forward more than a decade ago [1,2]. In particular, $5d$ transition metal compounds provide a platform to explore the rich physics stemming from the strong spin-orbit interaction and the relatively large spatial extension of atomic orbitals: The former admixes orbitals of different symmetry and gives rise to entangled spin and orbital magnetic moments; the latter attenuates electronic correlations and promotes covalency. Their combination produces an intricate network of interactions, comparable in strength, that connects all electronic degrees of freedom [3]. So far, much of the work has concentrated on the study of entangled spin-orbital states in systems with different band fillings and on multiple bond geometries motivated by the number of exotic electronic and magnetic interactions they give rise to [4–7]. However, little attention has been paid to other, equally intriguing effects, such as the coupling of electronic degrees of freedom to the lattice [8–10]. A number of theoretical predictions suggests that electron-lattice coupling is relevant for spin-orbit Mott insulators, particularly in cubic $5d^1$ systems: Indeed, in the limit of a very large crystal field, high-energy e_g states do not mix in, and otherwise degenerate t_{2g} states are split by spin-orbit coupling into an empty $j_{\mathrm{eff}} = 1/2$ Kramers doublet and a singly occupied $j_{\mathrm{eff}} = 3/2$ quartet, consisting of *two* Kramers doublets; the extra double degeneracy leads to Jahn-Teller (JT) instabilities and generates strong quantum effects [10]. In the specific case of double perovskite Ba_2NaOsO_6 [11], it was theoretically predicted that electron-lattice coupling results in entangled spin-orbital-lattice states [12] featuring multiferroic effects [13].

The electronic structure of Ba_2NaOsO_6 is mostly determined by molecular orbitals of weakly interacting, allegedly undistorted OsO_6 octahedra, the Os ions having nominal Os^{7+} ($5d^1$) and local O_h site symmetry [14]. Density-functional theory (DFT) calculations show that electronic correlation cannot sustain an insulating behaviour by itself unless assisted by a sizable spin-orbit coupling, thus confirming the spin-orbit-coupled Mott insulating nature of Ba_2NaOsO_6 [15–17]. Noticeably, despite the magnetic moment for the single $5d^1$ electron occupying the $j_{\mathrm{eff}} = 3/2$ states should be zero by virtue of

*Contact author: stefano.agrestini@diamond.ac.uk
†Contact author: marco.moretti@polimi.it

the exact cancellation of its spin and orbital angular momenta [18–20], Ba_2NaOsO_6 features an effective magnetic moment $\mu_{\text{eff}} \approx 0.6\mu_B$ in the paramagnetic phase [14,21] and a net moment of $0.2\mu_B$ in the long-range ordered canted antiferromagnetic (cAFM) phase below $T_N = 6.8$ K [11,14]. Recent DFT calculations show that this exotic magnetic order is understood and originates from the anomalous Dzyaloshinskii-Moriya interaction generated by JT distortions [22]. But, why is Ba_2NaOsO_6 magnetic at all to start with? More DFT and *ab initio* calculations suggest that the sizable magnetic moment found experimentally could be explained by strong Os $5d$–O $2p$ hybridization [12,16,23] and/or by the JT effect [12,13,15] but are not backed up by experiments: NMR [21,24], specific heat, and magnetization [25] data evidence a broken symmetry phase up to only a few degrees Kelvin above the magnetic transition, while x-ray [14] and neutron [26] diffraction and EXAFS experiments [27] show that the space group symmetry of Ba_2NaOsO_6 ($Fm\bar{3}m$) is cubic at higher temperatures, with no evidence of JT distortions. The sole experimental hint about a possible room temperature splitting of the $j_{\text{eff}} = 3/2$ quartet into two Kramers doublets comes from specific heat measurements [14]. The mismatch between theoretical predictions and experimental evidence calls for further investigations.

In this Letter, we address the question related to the origin of magnetism in Ba_2NaOsO_6 by spectroscopic methods sensitive to the bulk electronic structure and magnetic state of the Os ions, namely, resonant inelastic x-ray scattering (RIXS), x-ray absorption spectroscopy (XAS), and magnetic circular dichroism (XMCD). The analysis of our experimental results, supported by multiplet ligand-field theory (MLFT) calculations, shows that covalency increases the occupancy of the $5d$ states well beyond the nominal d^1 configuration and provides solid experimental evidence of a JT distortion in this system already at room temperature. In order to reconcile our and previous results, a dynamic mechanism for the JT distortion is proposed.

The synthesis of powder samples of Ba_2NaOsO_6 is described in Ref. [27], while single crystals are the same as in Ref. [24]. Os L_3 edge RIXS measurements were collected at beam line ID20 [28] at the European Synchrotron Radiation Facility (ESRF), O K edge RIXS measurements at I21 beam line [29] at the Diamond Light Source (DLS), and Os $L_{2,3}$ edge XAS and XMCD measurements at beam line P09 [30,31] at PETRA III at DESY. MLFT calculations on an OsO_6 cluster were carried out with QUANTY [32–34], which explicitly takes into account the full atomic multiplet, including spin-orbit coupling, and crystal field splitting acting on the metal and on the ligand ions, as well as their hybridization.

Figure 1(b) shows the Os L_3 edge RIXS map of powder Ba_2NaOsO_6 at 300 K, measured with a low-energy-resolution, high-throughput setup over a large range of incident and emitted photon energies in order to obtain a broad overview of the RIXS response in this system. The RIXS map is very rich, and, besides the elastic line at zero energy loss, a number of Raman-like excitations are clearly visible, resonating at incident photon energies roughly corresponding to the two peaks in the XAS profile [black curve in Fig. 3(a)]. The main excitations (labeled B, C, D, and E) are better appreciated in the two spectra in Fig. 1(a), obtained by cutting the RIXS map at constant incident photon energies. We note that (i) peaks B (0.51 ± 0.02 eV) and C (4.86 ± 0.21 eV) are relatively weak, compared to peaks D (6.55 ± 0.11 eV) and E (11.05 ± 0.10 eV)—however, their energy separation (4.35 and 4.50 eV, respectively) is very similar; (ii) peaks B and D resonate at 10.8734 keV, while peaks C and E resonate at 10.8778 keV, i.e., 4.40 eV higher in energy; (iii) the energy separation between peaks D and B and between peaks C and E (6.04 and 6.19 eV, respectively) is also very similar. The natural interpretation of all these features is in terms of ligand-field transitions; in particular, we assign peaks B and C to transitions within the Os $5d$ states, involving t_{2g} and e_g states, respectively, while peaks D and E to transitions from O $2p$ to Os $5d$ states, again involving t_{2g} and e_g states, respectively. We term the former *d-d* and the latter *charge-transfer* (CT) excitations and note that, unlike other compounds, e.g., cuprates [35], the fact that CT overwhelms *d-d* transitions suggests a strong covalent nature of the Os—O bond in Ba_2NaOsO_6.

Simulated RIXS spectra for optimal values of the parameters [36] are shown in Fig. 1(c) after convolution with the instrumental energy resolution for an appropriate

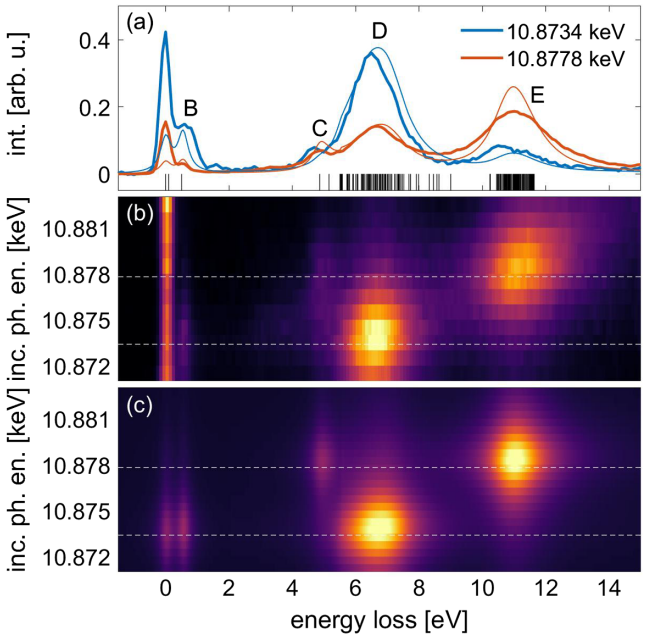

FIG. 1. (a) Experimental (thick) and simulated (thin lines) Os L_3 edge RIXS spectra of powder Ba_2NaOsO_6 at 300 K measured at selected incident photon energies, as extracted from the RIXS map of (b) and (c), respectively, at incident photon energies corresponding to the white dashed lines. Calculations of the excitation energies, vertical lines in the bottom of (a), and intensities were performed by MLFT, as explained in the text.

comparison with the experiments. The simulations reproduce the experimental data remarkably well, including the energies of the various excitations, their relative intensities, and the differences in their resonant behavior. In particular, MLFT calculations confirm the assignment above: In analogy to K_2TaCl_6 and Rb_2TaCl_6 [37], peak B is associated to the $j_{\mathrm{eff}} = 3/2$-to-$j_{\mathrm{eff}} = 1/2$ transition, whose energy is primarily set by the spin-orbit coupling constant, while peak C to t_{2g}-to-e_g transitions and its energy corresponds to the effective splitting of the t_{2g} and e_g orbitals (10 $\mathrm{Dq}^{\mathrm{eff}} = 4.9$ eV), resulting from both the ionic and covalent nature of the bonding. Information on the degree of covalency of the system is best extracted from CT transitions (peaks D and E); their energies and intensities are mostly influenced by the strength of the Os $5d$–O $2p$ hybridization and the CT energy: We find charge-transfer energy $\Delta = -4$ eV, classifying Ba_2NaOsO_6 as a negative charge-transfer system [38,39]. Remarkably, in order to reproduce the relative intensities of d-d and CT excitations, it has been necessary to expand the MLFT ground state wave function to include configurations with up to four ligand holes, i.e.,

$$|\Psi\rangle = \sum_{i=1}^{5} \alpha_i |5d^i \underline{L}^{i-1}\rangle, \tag{1}$$

where $\underline{L}$ denotes a ligand hole and $\sum_{i=1}^{5} |\alpha_i|^2 = 1$. We find that the nominal $5d^1$ configuration is negligible (0.01%), while the $5d^2\underline{L}$ (8.5%), $5d^3\underline{L}^2$ (29.0%), $5d^4\underline{L}^3$ (41.6%), and $5d^5\underline{L}^4$ (20.9%) configurations are dominant. Ultimately, the number of electrons effectively populating the Os $5d$ states is $n_d = \sum_{i=1}^{5} i|\alpha_i|^2 = 3.75$, meaning that almost three electrons are transferred from the O ligands to the central Os ion. This significant transfer of charge is consistent with DFT calculations, which report an even higher population of the Os $5d$ states, i.e., $n_d \approx 5$–6 [17].

Figure 2(a) shows the Os L_3 edge RIXS spectra of a Ba_2NaOsO_6 single crystal at 300 K, measured with a low-throughput, high-energy-resolution setup as a function of momentum transfer in a small energy range close to the elastic line at 10.8734 keV incident photon energy. Both the elastic line and peak B are slightly asymmetric, and peak B shows no momentum transfer dependence. The latter observation is consistent with the assumption that the electronic structure of Ba_2NaOsO_6 is mostly determined by molecular orbitals of weakly interacting, OsO_6 octahedra [14], thus justifying the use of MLFT calculations to perform a quantitative analysis of the experimental RIXS spectra and extract significant physical parameters.

So far, our experimental results support the notion that the electronic structure of Ba_2NaOsO_6 is mostly determined by the molecular orbitals of undistorted OsO_6 octahedra. The main challenge to this paradigm comes from O K edge RIXS and Os $L_{2,3}$ edge XMCD measurements. Figure 2(b) shows O K edge RIXS spectra of a Ba_2NaOsO_6 single crystal, collected at various

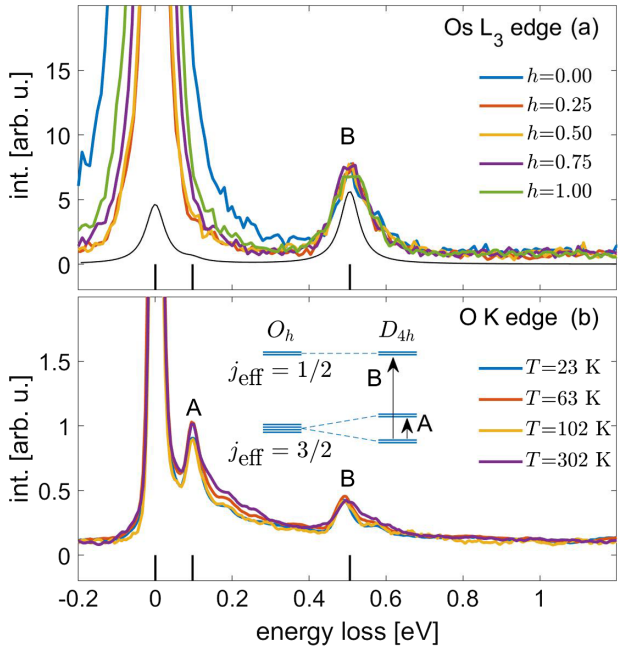

FIG. 2. (a) Os L_3 edge RIXS spectra of Ba_2NaOsO_6 single crystal at 300 K as a function of the transferred momentum along the $(10 + h, 0, 0)$ r.l.u. direction in reciprocal space. The thin black line shows the simulated RIXS spectrum in the experimental geometry corresponding to (10.5,0,0) r.l.u. momentum transfer. (b) O K edge RIXS spectra of powder Ba_2NaOsO_6 as a function of the temperature. Calculations of the excitation energies, vertical lines in (a) and (b), were performed by MLFT, as explained in the text. The inset in (b) shows the energy diagram of t_{2g} states split by spin-orbit coupling in O_h and D_{4h} symmetry.

temperatures in the range 21–302 K. Peak B is visible and accompanied by a weak satellite at higher energy; in addition, we find a sharp excitation at 0.095 ± 0.004 eV (labeled A), which shows neither systematic temperature nor momentum transfer dependence (see [40]), therefore excluding its magnetic or phononic origin. Peak A lies on top of a broad distribution of spectral weight extending from the elastic line up to approximately 0.4 eV, which can possibly arise from multiphonon excitations resonating at approximately 1 eV higher incident photon energy with respect to peak A (see [40]). Its most plausible interpretation is in terms of a d-d excitation and implies the breaking of the octahedral (O_h) site symmetry and the lifting of the $j_{\mathrm{eff}} = 3/2$ degeneracy into two doublets, between which RIXS transitions can occur [inset in Fig. 2(b)].

In order to further assess the nature of peak A and test the hypothesis of the breaking of the Os site symmetry to lower than octahedral, e.g., tetragonal (D_{4h}), we performed XMCD measurements in both the cAFM and paramagnetic phase. Os $L_{2,3}$ edge XAS and XMCD data measured at 3.5 K in a 5 T magnetic field are reported as continuous black lines in Figs. 3(a) and 3(b). The spectra at 40 K (see [40]) are qualitatively similar but with reduced intensity. We highlight the unusual simultaneous occurrence of two

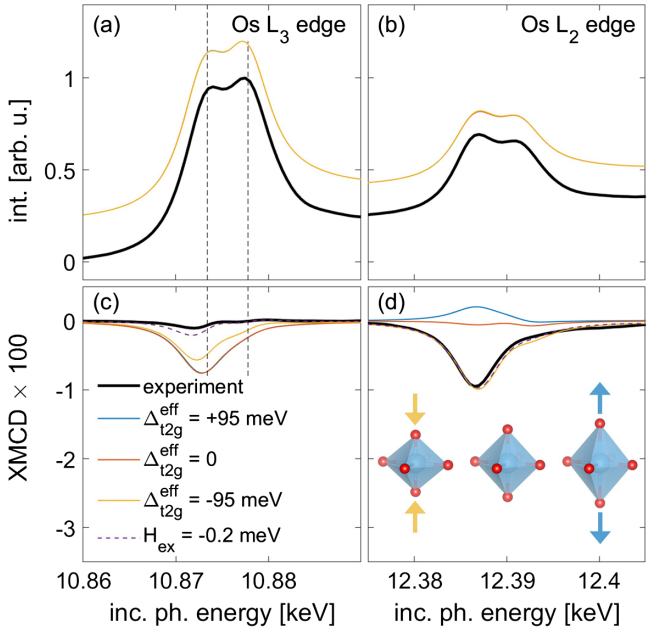

FIG. 3. Os L_3 (a),(c) and L_2 (b),(d) edge XAS and XMCD curves at 3.5 K. The thick black and thin colored lines correspond to experimental and simulated curves, respectively, normalized to the maximum of the L_3 absorption edge. The vertical dashed lines in (a) and (c) correspond to the incident photon energies used to measure and simulate the RIXS spectra in Fig. 1(a). The inset in (d) shows compressed, undistorted, and elongated OsO_6 octahedra, which refer to the simulated yellow, red, and blue curves, respectively. Note that the blue and orange curves almost perfectly overlap in (c).

features: First, the XMCD signal is negative at both L_3 and L_2 edges. The identical sign of XMCD at both edges suggests that the strength of the orbital magnetic moment contributes substantially to the total moment [44]. A similar effect has also been seen in the XMCD spectra of another $5d^1$ double perovskite material, Ba_2ZnReO_6 [26]; second, most of the XMCD intensity is at the L_2 absorption edge. A similar behavior has been observed by Veiga *et al.* in Ca_2FeOsO_6 and Sr_2FeOsO_6, where the (negative) XMCD signal at the L_2 edge is stronger than the (positive) XMCD signal at the L_3 edge [45]. In our case, the (negative) XMCD signal at the L_2 edge is much (approximately 15 times) smaller than the (negative) XMCD signal at the L_3 edge. The analysis of XMCD data based on sum rules [46,47] reveals a $L/2S_{\mathrm{eff}}$ ratio of -0.369 (see [40]), implying that the orbital and spin magnetic moments have opposite sign but different magnitude, thus preventing the cancellation of the magnetic moment, which remains finite. In order to clarify the origin of this behavior, we then performed MLFT calculations with the same parameters used to simulate the Os L_3 edge RIXS data above but varying the tetragonal crystal field $\Delta_{t2g}^{\mathrm{ion}}$, which results in an effective splitting of the t_{2g} states of $\Delta_{t2g}^{\mathrm{eff}}$ (see [40]). In the case of O_h symmetry [$\Delta_{t2g}^{\mathrm{eff}} = \Delta_{t2g}^{\mathrm{ion}} = 0$, red curves in Figs. 3(c) and 3(d)], the simulation predicts a strong XMCD signal at the Os L_3 edge and a weak one at L_2, in stark contrast to the experiments. Only the introduction of a negative tetragonal crystal field changes qualitatively the shape of the XMCD curves and considerably improves the agreement between simulated and experimental spectra (see [40]): The best agreement to the L_2 edge XMCD signal is obtained for $\Delta_{t2g}^{\mathrm{eff}} = -0.095$ eV ($\Delta_{t2g}^{\mathrm{ion}} = -0.25$ eV), which nicely matches the energy of peak A in O K edge RIXS [Fig. 2(b)]. It corresponds to a tetragonal compressive distortion of the OsO_6 octahedra along the z axis, which, in the absence of spin-orbit coupling, would lower the energy of the xy orbital to below that of the yz and zx orbitals. It is important to note that the simulated intensity of peak A for the proposed tetragonal distortion is too weak to be detected by Os L_3 edge RIXS [thin black line in Fig. 2(a)].

In essence, O K edge RIXS and Os $L_{2,3}$ edge XMCD measurements provide compelling evidence that Ba_2NaOsO_6 is JT active at all temperatures. On the one hand, our results agree with heat capacity measurements (JT distortions split the $j_{\mathrm{eff}} = 3/2$ states into two Kramers doublets, hence the integrated entropy through the magnetic phase transition of $R\ln 2$) [14], quantitatively reproduce the temperature dependence of the magnetic susceptibility in the paramagnetic phase (see Fig. 4), and support theoretical calculations for Ba_2NaOsO_6 [12,13]; on the other hand, they seemingly contradict x-ray diffraction [14], NMR [24,48], and EXAFS [27] studies, although a tetragonal distortion could not be ruled out by neutron diffraction [26]. In order to reconcile our and previous experiments, we speculate that Ba_2NaOsO_6 is subject to a dynamic JT effect: The system resonates between equivalent minima of the adiabatic potential energy surface (corresponding to different directions of the distortions), such that the average crystal structure remains undistorted, explaining why such

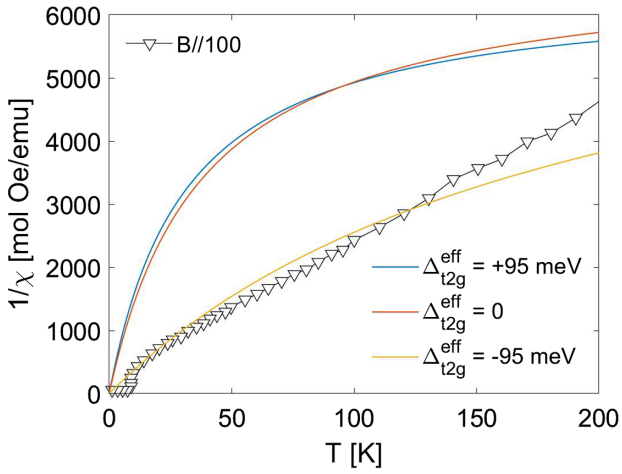

FIG. 4. Experimental (open triangles, from Ref. [14]) and simulated (continuous lines) inverse magnetic susceptibility of $Ba_2NaCaOsO_6$ as a function of the temperature.

distortions could not be observed directly by structural probes [49]. Moreover, its dynamical nature makes the JT distortion invisible to slow spectroscopic probes [49], such as NMR. Recently, signatures of dynamic JT effect were also found in the A_2MgReO_6 (A = Ca, Sr, and Ba) family, i.e., the Re analog of Ba_2NaOsO_6 [50].

Next, we calculate the expectation values of the magnetic moment (μ) at $T = 20$ K (paramagnetic phase) within MLFT (see [40]) to clarify the role of the various interactions in determining the magnetic properties of Ba_2NaOsO_6. In O_h symmetry, we find that for 10 Dq^{eff} = ∞ the $L_x/2S_x$ ratio is -1.00, meaning that the spin and orbital angular momenta are equal in size and have opposite sign, such that none of the $j_{eff} = 3/2$ states are magnetic ($\mu_x = 0$); but for a realistic, although large value of 10 Dq^{eff} (4.9 eV), a strong spin-orbit coupling mixes the $j_{eff} = 3/2$ ($m_j = \pm 3/2$) and the e_g inducing a finite magnetic moment ($\mu_x = 0.007\mu_B$). Covalency causes a partial suppression of the orbital angular moment, so that the magnetic moment reduces to $\mu_x = 0.004\mu_B$. Lowering the symmetry from O_h to D_{4h} due to a finite value of Δ_{t2g}^{eff} (-0.095 eV) has an important effect: The xy plane becomes an easy plane of magnetization, and the magnetic moment is increased with respect to the O_h case to $\mu_x = 0.014\mu_B$ in the presence of covalency. Also, the calculated value for $L/2S_{eff}$ is -0.375, which perfectly matches the experimental estimate from sum rules analysis of XMCD data (see [40]).

The simulation of the small XMCD signal at the Os L_3 edge remains unsatisfactory at this stage but can be improved, as explained in the following. The tetragonal compressive distortion of the OsO_6 octahedra [sketched in the inset in Fig. 3(d)] favors the alignment of the magnetic moments in the xy plane, consistent with the magnetic structure proposed in Ref. [24]. It turns out that in this case the XMCD signal at the Os L_3 edge is very sensitive to the presence of magnetic couplings between the Os ions; in particular, a fairly good agreement can be obtained by introducing an exchange field H_{ex} that mimics at a mean field level the weak antiferromagnetic coupling between nearest-neighbor magnetic moments. The best simulation is obtained for -0.2 meV [dashed purple curves in Figs. 3(c) and 3(d)], which roughly compares to the ordering temperature ($k_B T_N \approx 0.6$ meV) [14], thus strengthening the intuition that the reduced Os L_3 edge XMCD intensity originates from Os-Os magnetic interactions.

In summary, our spectroscopic investigations provide a quantitative estimate of the relevant electronic interactions in Ba_2NaOsO_6; all together, they account for its finite magnetic moment and solve the puzzle concerning the origin of magnetism in this material. In particular, spin-orbit coupling and dynamic JT effects, which RIXS is sensitive to [51], entangle the spin, orbit, and lattice degrees of freedom and could give rise to exotic magnetic (and vibronic) orders [52]. Beyond the specific case of Ba_2NaOsO_6, our results are relevant for several (anti) ferromagnetic double perovskites with nominal $4d^1$ [53,54] and $5d^1$ [37,54–57] electronic configuration, as well as other systems with exotic magnetic ground states [58–60].

Acknowledgments—We acknowledge Ian Fisher for providing the single crystalline samples. We acknowledge the ESRF (Grenoble, France), DLS (Didcot, United Kingdom), and DESY (Hamburg, Germany), a member of the Helmholtz Association HGF, for provision of synchrotron radiation facilities. Parts of this research were carried out at beam line ID20 at ESRF under Proposals No. HC-4277 and No. HC-4912. We thank F. Gerbon for assistance and support in using the beam line. Parts of this research were carried out at beam line P09 at PETRA III under Proposal No. I-20200367EC. We thank Dr. J. R. Linares Mardegan and Dr. T. Pohlmann for their help with the measurements and Dr. Olaf Leupold for assistance in cooling down and operating the 6T/2T/2T magnet at P09. The 6T/2T/2T magnet used for the XMCD measurements was funded in part by the BMBF Grant No. 05K2013 from the German Federal Ministry of Education and Research. The work here presented is partly funded by the European Union—Next Generation EU—"PNRR—M4C2, investimento 1.1—Fondo PRIN 2022"—"Superlattices of relativistic oxides" (ID No. 2022L28H97, CUP D53D23002260006) and "Spin-charge-lattice coupling in relativistic Mott insulators" (ID No. 202243JHMW, CUP J53D23001350006), and by the U.S. National Science Foundation (NSF) Grant No. DMR-1905532 (V. F. M.) and NSF Materials Research Science and Engineering Center (MRSEC) Grant No. DMR-2011876 (P. M. W.).

[1] B. J. Kim, H. Jin, S. J. Moon, J.-Y. Kim, B.-G. Park, C. S. Leem, J. Yu, T. W. Noh, C. Kim, S.-J. Oh, J.-H. Park, V. Durairaj, G. Cao, and E. Rotenberg, Novel $J_{eff} = 1/2$ Mott state induced by relativistic spin-orbit coupling in Sr_2IrO_4, Phys. Rev. Lett. **101**, 076402 (2008).

[2] B. J. Kim, H. Ohsumi, T. Komesu, S. Sakai, T. Morita, H. Takagi, and T. Arima, Phase-sensitive observation of a spin-orbital Mott state in Sr_2IrO_4, Science **323**, 1329 (2009).

[3] W. Witczak-Krempa, G. Chen, Y. B. Kim, and L. Balents, Correlated quantum phenomena in the strong spin-orbit regime, Annu. Rev. Condens. Matter Phys. **5**, 57 (2014).

[4] G. Jackeli and G. Khaliullin, Mott insulators in the strong spin-orbit coupling limit: From Heisenberg to a quantum compass and Kitaev models, Phys. Rev. Lett. **102**, 017205 (2009).

[5] J. G. Rau, E. K.-H. Lee, and H.-Y. Kee, Spin-orbit physics giving rise to novel phases in correlated systems: Iridates and related materials, Annu. Rev. Condens. Matter Phys. **7**, 195 (2016).

[6] S. M. Winter, A. A. Tsirlin, M. Daghofer, J. van den Brink, Y. Singh, P. Gegenwart, and R. Valentí, Models and materials for generalized Kitaev magnetism, J. Phys. Condens. Matter **29**, 493002 (2017).

[7] G. Cao and P. Schlottmann, The challenge of spin–orbit-tuned ground states in iridates: A key issues review, Rep. Prog. Phys. **81**, 042502 (2018).

[8] H. Liu and G. Khaliullin, Pseudo-Jahn-Teller effect and magnetoelastic coupling in spin-orbit Mott insulators, Phys. Rev. Lett. **122**, 057203 (2019).

[9] S. V. Streltsov and D. I. Khomskii, Jahn-Teller effect and spin-orbit coupling: Friends or foes?, Phys. Rev. X **10**, 031043 (2020).

[10] S. V. Streltsov, F. V. Temnikov, K. I. Kugel, and D. I. Khomskii, Interplay of the Jahn-Teller effect and spin-orbit coupling: The case of trigonal vibrations, Phys. Rev. B **105**, 205142 (2022).

[11] K. E. Stitzer, M. D. Smith, and H.-C. zur Loye, Crystal growth of Ba_2MOsO_6 (M = Li, Na) from reactive hydroxide fluxes, Solid State Sci. **4**, 311 (2002).

[12] L. Xu, N. Bogdanov, A. A Princep, P. Fulde, J. van den Brink, and L. Hozoi, Covalency and vibronic couplings make a nonmagnetic $j = 3/2$ ion magnetic, npj Quantum Mater. **1**, 16029 (2016).

[13] N. Iwahara, V. Vieru, and L. F. Chibotaru, Spin-orbital-lattice entangled states in cubic d^1 double perovskites, Phys. Rev. B **98**, 075138 (2018).

[14] A. S. Erickson, S. Misra, G. J. Miller, R. R. Gupta, Z. Schlesinger, W. A. Harrison, J. M. Kim, and I. R. Fisher, Ferromagnetism in the Mott insulator Ba_2NaOsO_6, Phys. Rev. Lett. **99**, 016404 (2007).

[15] H. J. Xiang and M.-H. Whangbo, Cooperative effect of electron correlation and spin-orbit coupling on the electronic and magnetic properties of Ba_2NaOsO_6, Phys. Rev. B **75**, 052407 (2007).

[16] K.-W. Lee and W. E. Pickett, Orbital-quenching–induced magnetism in Ba_2NaOsO_6, Europhys. Lett. **80**, 37008 (2007).

[17] R. Cong, R. Nanguneri, B. Rubenstein, and V. F. Mitrović, Evidence from first-principles calculations for orbital ordering in Ba_2NaOsO_6: A Mott insulator with strong spin-orbit coupling, Phys. Rev. B **100**, 245141 (2019).

[18] M. Kotani, On the magnetic moment of complex ions (I), J. Phys. Soc. Jpn. **4**, 293 (1949).

[19] A. Abragam and B. Bleaney, *Electron Paramagnetic Resonance of Transition Ions* (Clarendon Press, Oxford, 1970), pp. 417–426.

[20] F. E. Mabbs and D. J. Machin, *Magnetism and Transition Metal Complexes* (Chapman and Hall, London, 1973), pp. 68–84.

[21] R. Cong, E. Garcia, P. C. Forino, A. Tassetti, G. Allodi, A. P. Reyes, P. M. Tran, P. M. Woodward, C. Franchini, S. Sanna, and V. F. Mitrović, Effects of charge doping on Mott insulator with strong spin-orbit coupling, $Ba_2Na_{1-x}Ca_xOsO_6$, Phys. Rev. Mater. **7**, 084409 (2023).

[22] D. Fiore Mosca, L. V. Pourovskii, B. H. Kim, P. Liu, S. Sanna, F. Boscherini, S. Khmelevskyi, and C. Franchini, Interplay between multipolar spin interactions, Jahn-Teller effect, and electronic correlation in a $J_{\text{eff}} = \frac{3}{2}$ insulator, Phys. Rev. B **103**, 104401 (2021).

[23] K.-H. Ahn, K. Pajskr, K.-W. Lee, and J. Kuneš, Calculated g-factors of $5d$ double perovskites Ba_2NaOsO_6 and Ba_2YOsO_6, Phys. Rev. B **95**, 064416 (2017).

[24] L. Lu, M. Song, W. Liu, A. P. Reyes, P. Kuhns, H. O. Lee, I. R. Fisher, and V. F. Mitrović, Magnetism and local symmetry breaking in a Mott insulator with strong spin orbit interactions, Nat. Commun. **8**, 14407 (2017).

[25] K. Willa, R. Willa, U. Welp, I. R. Fisher, A. Rydh, W.-K. Kwok, and Z. Islam, Phase transition preceding magnetic long-range order in the double perovskite Ba_2NaOsO_6, Phys. Rev. B **100**, 041108(R) (2019).

[26] V. da Cruz Pinha Barbosa, J. Xiong, P. M. Tran, M. A. McGuire, J. Yan, M. T. Warren, R. V. Aguilar, W. Zhang, M. Randeria, N. Trivedi, D. Haskel, and P. M. Woodward, The impact of structural distortions on the magnetism of double perovskites containing $5d^1$ transition-metal ions, Chem. Mater. **34**, 1098 (2022).

[27] J. K. Kesavan, D. Fiore Mosca, S. Sanna, F. Borgatti, G. Schuck, P. M. Tran, P. M. Woodward, V. F. Mitrović, C. Franchini, and F. Boscherini, Doping evolution of the local electronic and structural properties of the double perovskite $Ba_2Na_{1-x}Ca_xOsO_6$, J. Phys. Chem. C **124**, 16577 (2020).

[28] M. Moretti Sala, K. Martel, C. Henriquet, A. Al Zein, L. Simonelli, C. J. Sahle, H. Gonzalez, M.-C. Lagier, C. Ponchut, S. Huotari, R. Verbeni, M. Krisch, and G. Monaco, A high-energy-resolution resonant inelastic x-ray scattering spectrometer at ID20 of the European Synchrotron Radiation Facility, J. Synchrotron Radiat. **25**, 580 (2018).

[29] K.-J. Zhou, A. Walters, M. Garcia-Fernandez, T. Rice, M. Hand, A. Nag, J. Li, S. Agrestini, P. Garland, H. Wang, S. Alcock, I. Nistea, B. Nutter, N. Rubies, G. Knap, M. Gaughran, F. Yuan, P. Chang, J. Emmins, and G. Howell, I21: An advanced high-resolution resonant inelastic x-ray scattering beamline at Diamond Light Source, J. Synchrotron Radiat. **29**, 563 (2022).

[30] J. Strempfer, S. Francoual, D. Reuther, D. K. Shukla, A. Skaugen, H. Schulte-Schrepping, T. Kracht, and H. Franz, Resonant scattering and diffraction beamline P09 at PETRA III, J. Synchrotron Radiat. **20**, 541 (2013).

[31] J. Strempfer, J. R. L. Mardegan, S. Francoual, L. S. I. Veiga, L. Bouchenoire, T. Spitzbart, and H. Zink, Fast helicity switching of x-ray circular polarization at beamline P09 at PETRA III, AIP Conf. Proc. **1741**, 030017 (2016).

[32] M. W. Haverkort, M. Zwierzycki, and O. K. Andersen, Multiplet ligand-field theory using Wannier orbitals, Phys. Rev. B **85**, 165113 (2012).

[33] Y. Lu, M. Höppner, O. Gunnarsson, and M. W. Haverkort, Efficient real-frequency solver for dynamical mean-field theory, Phys. Rev. B **90**, 085102 (2014).

[34] M. W. Haverkort, G. Sangiovanni, P. Hansmann, A. Toschi, Y. Lu, and S. Macke, Bands, resonances, edge singularities and excitons in core level spectroscopy investigated within the dynamical mean-field theory, Europhys. Lett. **108**, 57004 (2014).

[35] M. M. Sala, V. Bisogni, C. Aruta, G. Balestrino, H. Berger, N. B. Brookes, G. M. de Luca, D. D. Castro, M. Grioni, M. Guarise, P. G. Medaglia, F. M. Granozio, M. Minola, P. Perna, M. Radovic, M. Salluzzo, T. Schmitt, K. J. Zhou, L. Braicovich, and G. Ghiringhelli, Energy and symmetry of dd excitations in undoped layered cuprates measured by

Cu L_3 resonant inelastic x-ray scattering, New J. Phys. **13**, 043026 (2011).

[36] OsO_6 cluster parameters [eV]: $U_{dd} = 1.0$, $U_{pd} = 3.0$, charge transfer energy $\Delta_{CT} = -4.0$, spin-orbit coupling $\lambda = 0.41$, ionic crystal field $10\,\mathrm{Dq}^{\mathrm{ion}} = 3.3$, $\Delta^{\mathrm{ion}}_{t_{2g}} = -0.25$, and $\Delta^{\mathrm{ion}}_{e_g} = -0.5$, hybridization $V(e_g) = 6.2$ and $V(t_{2g}) = 3.5$, and ligand crystal field $10\,\mathrm{Dq}^{\mathrm{lig}} = 0.95$. Slater integrals were reduced to 70% of the Hartree-Fock values. For all simulations, we have considered the thermal population of the electronic state using the Boltzmann distribution.

[37] H. Ishikawa, T. Takayama, R. K. Kremer, J. Nuss, R. Dinnebier, K. Kitagawa, K. Ishii, and H. Takagi, Ordering of hidden multipoles in spin-orbit entangled $5d^1$ Ta chlorides, Phys. Rev. B **100**, 045142 (2019).

[38] T. Mizokawa, H. Namatame, A. Fujimori, K. Akeyama, H. Kondoh, H. Kuroda, and N. Kosugi, Origin of the band gap in the negative charge-transfer-energy compound $NaCuO_2$, Phys. Rev. Lett. **67**, 1638 (1991).

[39] D. Khomskii, Unusual valence, negative charge-transfer gaps and self-doping in transition-metal compounds, arXiv:cond-mat/0101164.

[40] See Supplemental Material at http://link.aps.org/supplemental/10.1103/PhysRevLett.133.066501 for further information, which includes Refs. [41–43].

[41] C. Piamonteze, P. Miedema, and F. M. F. de Groot, Accuracy of the spin sum rule in XMCD for the transition-metal l edges from manganese to copper, Phys. Rev. B **80**, 184410 (2009).

[42] M. A. Laguna-Marco, D. Haskel, N. Souza-Neto, J. C. Lang, V. V. Krishnamurthy, S. Chikara, G. Cao, and M. van Veenendaal, Orbital magnetism and spin-orbit effects in the electronic structure of $BaIrO_3$, Phys. Rev. Lett. **105**, 216407 (2010).

[43] M. A. Laguna-Marco, P. Kayser, J. A. Alonso, M. J. Martínez-Lope, M. van Veenendaal, Y. Choi, and D. Haskel, Electronic structure, local magnetism, and spin-orbit effects of Ir(IV)-, Ir(V)-, and Ir(VI)-based compounds, Phys. Rev. B **91**, 214433 (2015).

[44] A. Rogalev and F. Wilhelm, Magnetic circular dichroism in the hard x-ray range, Phys. Met. Metallogr. **116**, 1285 (2015).

[45] L. S. I. Veiga, G. Fabbris, M. van Veenendaal, N. M. Souza-Neto, H. L. Feng, K. Yamaura, and D. Haskel, Fragility of ferromagnetic double exchange interactions and pressure tuning of magnetism in $3d-5d$ double perovskite Sr_2FeOsO_6, Phys. Rev. B **91**, 235135 (2015).

[46] B. T. Thole, P. Carra, F. Sette, and G. van der Laan, X-ray circular dichroism as a probe of orbital magnetization, Phys. Rev. Lett. **68**, 1943 (1992).

[47] P. Carra, B. T. Thole, M. Altarelli, and X. Wang, X-ray circular dichroism and local magnetic fields, Phys. Rev. Lett. **70**, 694 (1993).

[48] W. Liu, R. Cong, A. P. Reyes, I. R. Fisher, and V. F. Mitrović, Nature of lattice distortions in the cubic double perovskite Ba_2NaOsO_6, Phys. Rev. B **97**, 224103 (2018).

[49] I. Bersuker, *The Jahn-Teller Effect* (Cambridge University Press, Cambridge, England, 2006), 10.1017/CBO9780511524769.

[50] F. I. Frontini, G. H. J. Johnstone, N. Iwahara, P. Bhattacharyya, N. A. Bogdanov, L. Hozoi, M. H. Upton, D. M. Casa, D. Hirai, and Y.-J. Kim, Spin-orbit-lattice entangled state in A_2MgReO_6 (A = Ca, Sr, Ba) revealed by resonant inelastic x-ray scattering, Phys. Rev. Lett. **133**, 036501 (2024).

[51] N. Iwahara and S. Shikano, Vibronic excitations in resonant inelastic x-ray scattering spectra of K_2RuCl_6, Phys. Rev. Res. **5**, 023051 (2023).

[52] N. Iwahara and L. F. Chibotaru, Vibronic order and emergent magnetism in cubic d^1 double perovskites, Phys. Rev. B **107**, L220404 (2023).

[53] T. Aharen, J. E. Greedan, C. A. Bridges, A. A. Aczel, J. Rodriguez, G. MacDougall, G. M. Luke, T. Imai, V. K. Michaelis, S. Kroeker, H. Zhou, C. R. Wiebe, and L. M. D. Cranswick, Magnetic properties of the geometrically frustrated $s = \frac{1}{2}$ antiferromagnets, La_2LiMoO_6 and Ba_2YMoO_6, with the b-site ordered double perovskite structure: Evidence for a collective spin-singlet ground state, Phys. Rev. B **81**, 224409 (2010).

[54] H. Ishikawa, T. Yajima, A. Matsuo, and K. Kindo, Ligand dependent magnetism of the $j_{\mathrm{eff}} = 3/2$ Mott insulator Cs_2MX_6 (M = Ta, Nb, X = Br, Cl), J. Phys. Condens. Matter **33**, 125802 (2021).

[55] A. J. Steele, P. J. Baker, T. Lancaster, F. L. Pratt, I. Franke, S. Ghannadzadeh, P. A. Goddard, W. Hayes, D. Prabhakaran, and S. J. Blundell, Low-moment magnetism in the double perovskites Ba_2MOsO_6 (m = Li, Na), Phys. Rev. B **84**, 144416 (2011).

[56] K. Yamamura, M. Wakeshima, and Y. Hinatsu, Structural phase transition and magnetic properties of double perovskites Ba_2CaMO_6 (M = W, Re, Os), J. Solid State Chem. **179**, 605 (2006).

[57] A. Mansouri Tehrani and N. A. Spaldin, Untangling the structural, magnetic dipole, and charge multipolar orders in Ba_2MgReO_6, Phys. Rev. Mater. **5**, 104410 (2021).

[58] E. J. Cussen, D. R. Lynham, and J. Rogers, Magnetic order arising from structural distortion: Structure and magnetic properties of Ba_2LnMoO_6, Chem. Mater. **18**, 2855 (2006).

[59] C. R. Wiebe, J. E. Greedan, G. M. Luke, and J. S. Gardner, Spin-glass behavior in the $s = 1/2$ fcc ordered perovskite Sr_2CaO_6, Phys. Rev. B **65**, 144413 (2002).

[60] C. R. Wiebe, J. E. Greedan, P. P. Kyriakou, G. M. Luke, J. S. Gardner, A. Fukaya, I. M. Gat-Malureanu, P. L. Russo, A. T. Savici, and Y. J. Uemura, Frustration-driven spin freezing in the $s = 1/2$ fcc perovskite Sr_2MgReO_6, Phys. Rev. B **68**, 134410 (2003).